designs

MDPI

Article

Design and Development of a Low-Power IoT System for Continuous Temperature Monitoring

Luis Miguel Pires [1,2,*], João Figueiredo [1], Ricardo Martins [1], João Nascimento [1] and José Martins [1,3,*]

[1] Technologies and Engineering School (EET), Instituto Politécnico da Lusofonia (IPLuso), 1700-098 Lisbon, Portugal; a22311749@mso365.ipluso.pt (J.F.); a22408795@mso365.ipluso.pt (R.M.); a22409486@mso365.ipluso.pt (J.N.)
[2] Department of Electronical Engineering, Telecommunications and Computers (DEETC), Instituto Superior de Engenharia de Lisboa (ISEL), 1959-007 Lisbon, Portugal
[3] Department of Systems and Informatics (DSI), Setúbal School of Technology, Instituto Politécnico de Setúbal (IPS), Campus do IPS—Estefanilha, 2910-761 Setubal, Portugal
* Correspondence: luis.pires@ipluso.pt (L.M.P.); jose.manuel.martins@ipluso.pt (J.M.)

Abstract: This article presents the development of a compact, high-precision, and energy-efficient temperature monitoring system designed for tracking applications where continuous and accurate thermal monitoring is essential. Built around the HY0020 System-on-Chip (SoC), the system integrates two bandgap-based temperature sensors—one internal to the SoC and one external (Si7020-A20)—mounted on a custom PCB and powered by a coin cell battery. A distinctive feature of the system is its support for real-time parameterization of the internal sensor, which enables advanced capabilities such as thermal profiling, cross-validation, and onboard diagnostics. The system was evaluated under both room temperature and refrigeration conditions, demonstrating high accuracy with the internal sensor showing an average error of 0.041 °C and −0.36 °C, respectively, and absolute errors below ±0.5 °C. With an average current draw of just 0.01727 mA, the system achieves an estimated autonomy of 6.6 years on a 1000 mAh battery. Data are transmitted via Bluetooth Low Energy (BLE) to a Raspberry Pi 4 gateway and forwarded to an IoT cloud platform for remote access and analysis. With a total cost of approximately EUR 20 and built entirely from commercially available components, this system offers a scalable and cost-effective solution for a wide range of temperature-sensitive applications. Its combination of precision, long-term autonomy, and advanced diagnostic capabilities make it suitable for deployment in diverse fields such as supply chain monitoring, environmental sensing, biomedical storage, and smart infrastructure—where reliable, low-maintenance thermal tracking is essential.

Keywords: IoT; low-power sensing; temperature monitoring; bandgap sensor; sensor parameterization; SoC

Academic Editor: Bhanu Shrestha

Received: 20 May 2025
Revised: 5 June 2025
Accepted: 10 June 2025
Published: 12 June 2025

Citation: Pires, L.M.; Figueiredo, J.; Martins, R.; Nascimento, J.; Martins, J. Design and Development of a Low-Power IoT System for Continuous Temperature Monitoring. *Designs* **2025**, *9*, 73. https://doi.org/10.3390/designs9030073

1. Introduction

Temperature monitoring plays a critical role in logistics and tracking systems, particularly in preserving the integrity of temperature-sensitive products. This directly supports several United Nations Sustainable Development Goals (SDGs), including SDG 2 (Zero Hunger), SDG 3 (Good Health and Well-being), SDG 9 (Industry, Innovation, and Infrastructure), SDG 12 (Responsible Consumption and Production), and SDG 13 (Climate Action).

Temperature fluctuations can lead to spoilage of food and pharmaceuticals, posing risks to health and contributing to waste [1]. Effective cold-chain management reduces post-harvest losses and improves access to nutritious food, addressing hunger and food insecurity (SDG 2) [2]. In the pharmaceutical sector, maintaining thermal conditions, is essential to ensure the efficacy of vaccines and medicines, contributing to disease control (SDG 3) [3]. The adoption of IoT sensors enhances supply chain efficiency, reduces waste, and promotes sustainable consumption and production practices (SDG 12) [4]. Furthermore, smart logistics infrastructures improve resilience and sustainability by optimizing processes and minimizing environmental impacts (SDG 9) [5]. Failures in heat monitoring contribute not only to waste but also to increased carbon emissions from production and transportation [6], making advanced thermal tracking technologies essential for climate action (SDG 13) [7].

Aligned with these goals, the European Union has introduced the Digital Product Passport (DPP), a key initiative under the Eco-design for Sustainable Products Regulation [8,9]. The DPP promotes transparency and sustainability throughout the product life cycle by assigning each product a digital identity accessible via QR codes or similar technologies. Embedded sensors can contribute real-time temperature data to the DPP, offering a continuously updated view of a product's condition throughout its journey.

In this context, the internal temperature sensor embedded within the HY0020 System-on-Chip (SoC) (FDK, Tokyo, Japan) [10], based on the Nordic nRF52832 platform (Nordic Semiconductor, Trondheim, Norway) [11], distinguishes itself as a high-performance and energy-efficient component. It supports advanced functionalities such as real-time parameterization, thermal profiling, and background diagnostics—features that are seldom available in low-power embedded systems. These capabilities render it particularly suitable for applications requiring precise, autonomous, and long-term thermal monitoring.

To evaluate and characterize these features, a custom-designed printed circuit board (PCB) was developed, integrating the HY0020 SoC [10] alongside an external reference sensor (Si7020-A20, Silicon Labs, Austin, TX, USA) [12] and a third sensor (DHT22, Adafruit, New York, NY, USA) [13] and managed by an independent microcontroller. This architecture facilitates cross-validation, system-level diagnostics, and comprehensive thermal analysis, thereby enhancing the reliability and robustness of the measurements.

The proposed system, designated IoT-Temp Node, is intended for deployment across a diverse range of Internet of Things (IoT) domains, including cold-chain logistics, smart agriculture, environmental monitoring, intelligent infrastructure, and biomedical transport. Its compact design, extended operational autonomy, and low power consumption make it particularly well suited for long-term use in resource-constrained or difficult-to-access environments. Data collected by the system are transmitted via Bluetooth Low Energy (BLE) to a Raspberry Pi 4 (Raspberry Pi, Cambridge, UK) gateway [14], which subsequently forwards them to an IoT cloud platform for remote access and analysis.

The remainder of this article is structured as follows: Section 2 presents the background and related work; Section 3 describes the materials and methods; Section 4 discusses the results; and Section 5 concludes with future directions.

2. Background and Relevant Research

This section presents the theory, which forms the basis of this manuscript, with special emphasis on the bandgap voltage reference in Section 2.1. Section 2.2 presents research based on related works.

2.1. Background

Temperature measurement is a fundamental aspect of electronic systems and is commonly employed for monitoring, thermal regulation, and circuit protection. Temperature sensors can be broadly categorized into two types: internal sensors, which are integrated into microcontrollers (MCUs) or System-on-Chip (SoC) devices, and external sensors, which are implemented as discrete components.

Internal temperature sensors are typically embedded within microcontrollers or processors to monitor the chip's own temperature and prevent thermal damage. These sensors are generally based on semiconductor junctions, utilizing the temperature-dependent electrical characteristics of these materials [15]. While they offer advantages such as low cost and minimal power consumption, their accuracy is generally lower compared to external sensors.

External temperature sensors, on the other hand, are dedicated devices designed for higher precision and broader application flexibility [16]. These include thermistors (negative temperature coefficient—NTC—and positive temperature coefficient—PTC), bandgap-based sensors, thermocouples, and digital temperature sensors [16]. External sensors can be optimized for specific temperature ranges and are widely used in industrial, medical, and automotive applications due to their superior accuracy and configurability [17].

Among these, bandgap-based sensors are particularly notable for their stability and integration potential. A bandgap voltage reference is typically formed by subtracting the voltage of a forward-biased diode (or base-emitter junction), which has a negative temperature coefficient, from a voltage that is proportional to bsolute temperature (PTAT). The PTAT voltage is generated by amplifying the voltage difference between two forward-biased junctions operating at different current densities. A simplified representation of a bandgap voltage reference system is shown in Figure 1.

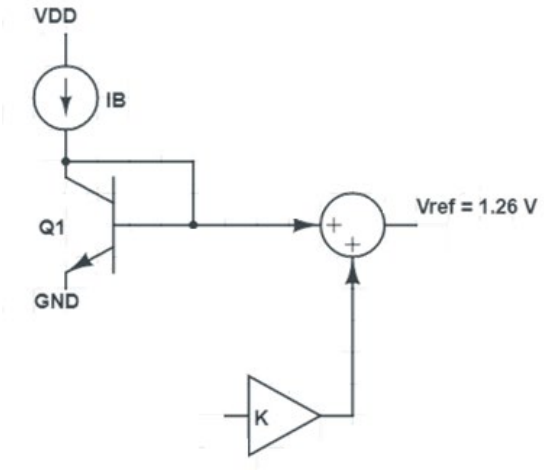

Figure 1. A simplified circuit of bandgap voltage reference (adapted from [16]).

A forward-biased base-emitter junction of a bipolar transistor has an I–V relationship given by [16,17]

$$I_C = I_S \cdot e^{q \cdot V_{BE}/k \cdot T} \quad (1)$$

where I_S is the transistor scale current and, although not shown, has a strong dependence on temperature [16,17]. Writing the base-emitter voltage as a function of collector current and temperature, it can be shown that [17]

$$V_{BE} = V_{G0} \cdot \left(1 - \frac{T}{T_0}\right) + V_{BE0} \cdot \frac{T}{T_0} + \frac{m \cdot k \cdot T}{q} \cdot \ln\left(\frac{T_0}{T}\right) + \frac{k \cdot T}{q} \cdot \ln\left(\frac{J_C}{J_{C0}}\right) \quad (2)$$

where V_{G0} is the bandgap voltage of silicon extrapolated to 0 °K (approximately 1.206 V [18]), k is Boltzmann's constant, and m is a temperature constant approximately equal to 2.3 [18]. The symbols J_c and T denote the collector current density and temperature, respectively, whereas the subscript 0 denotes an appropriate quantity at a reference temperature T_0 [17]. Specifically, J_{C0} is the collector current density at the reference temperature T_0, while J_c is that at the actual temperature T [17]. Similarly, V_{BE0} is the junction voltage for the reference temperature T_0, whereas V_{BE} is the base-emitter junction voltage for the actual temperature T [17]. Remember that the junction current relates to the junction current density according to the relation

$$I_C = A_E \cdot J_C \quad (3)$$

where A_E is the effective area of the base-emitter junction.

For the I_C constant, V_{BE} will have approximately a −2 mV/ºK temperature dependence around room temperature [18]. This negative temperature dependence is canceled by the PTAT temperature dependence of the amplified difference of two base-emitter junctions biased at fixed but different current densities [18]. Using (2), there are two base-emitter junctions biased at currents J_2 and J_1, and then, the difference in their junctions voltages is given by [18]

$$\Delta V_{BE} = V_2 - V_1 = \frac{k \cdot T}{q} \cdot \ln\left(\frac{J_2}{J_1}\right) \quad (4)$$

Thus, the difference in the junction voltages is proportional to the absolute temperature [17]. This proportionality is quite exact and remains so if the collector currents are temperature dependent if their ratio is fixed [17,18]. It will be considered shortly that, in a bandgap voltage reference, the output voltage appears temperature-independent, while the junction currents become proportional to absolute temperature (assuming temperature-independent resistors) [17,18]. Hence, to bear the derivations easier, we shall first assume that junction currents are proportional to the absolute temperature; later, we will examine the elaborations in [17,18]. Thus, we first assume that

$$\frac{J_i}{J_{i0}} = \frac{T}{T_0} \quad (5)$$

where J_i is the collector current density of the ith transistor, and J_{i0} is the diameter of the same current density at the reference temperature [17,18].

Now, let us assume that the smaller base-emitter voltage is multiplied by a factor K and then added to the larger base-emitter voltage [17,18]. Using (4), (5), and (2), we obtain

$$V_{ref} = V_{BE2} + K \cdot \Delta V_{BE} \quad (6)$$

$$V_{ref} = V_{G0} + \frac{T}{T_0} \cdot (V_{BE0-2} - V_{G0}) + (m-1) \cdot \frac{k \cdot T}{q} \cdot \ln\left(\frac{T_0}{T}\right) + K \cdot \frac{k \cdot T}{q} \cdot \ln\left(\frac{J_2}{J_1}\right) \quad (7)$$

Equation (7) is the fundamental equation giving the relationship between the output voltage of a bandgap voltage reference and temperature [18]. If we want this relationship to be zero at a particular temperature, we can differentiate (7) with respect to temperature and set the derivative to zero at the desired reference temperature. From (7), we have [18]

$$\frac{\partial V_{ref}}{\partial T} = \frac{1}{T_0} \cdot (V_{BE0-2} - V_{G0}) + K \cdot \frac{k}{q} \cdot \ln\left(\frac{J_2}{J_1}\right) + (m-1) \cdot \frac{k}{q} \cdot \left[\ln\left(\frac{T_0}{T}\right) - 1\right] \quad (8)$$

Setting (8) equal to zero at $T = T_0$, we see that for zero temperature dependence at the reference temperature, we need [18]

$$V_{BE0-2} + K \cdot \frac{k \cdot T_0}{q} \cdot \ln\left(\frac{J_2}{J_1}\right) = V_{G0} + (m-1) \cdot \frac{k \cdot T_0}{q} \quad (9)$$

The left side of (9) is the output voltage V_{ref} at $T = T_0$ from (7). Thus, for zero temperature dependence at $T = T_0$, we need [18]

$$V_{ref-0} = V_{G0} + (m-1) \cdot \frac{k \cdot T_0}{q} \tag{10}$$

For the special case of $T_0 = 300$ °K and m = 2.3 [18], (10) implies that,

$$V_{ref-0} = 1.24\,V$$

for zero temperature dependence. Notice that this value is independent of the reference current densities [17,18]. If a larger density is chosen, then K must be taken appropriately smaller to obtain the correct output reference voltage. In many integrated voltage references, this correct output voltage is obtained by trimming the device via a wafer test. From (9), value for K must be [17,18]

$$K = \frac{V_{G0} + (m-1) \cdot \frac{k \cdot T_0}{q} - V_{BE0-2}}{\frac{kT_O}{q} \ln\left(\frac{J_2}{J_1}\right)} = \frac{1.24 - V_{BE0-2}}{0.0258 \cdot \ln\left(\frac{J_2}{J_1}\right)} \tag{11}$$

at 300 °K.

Now, the reason for naming it the bandgap voltage should be apparent. The output of a bandgap voltage for zero temperature variation adds a small correction term to account for second-order effects [18,19].

The output of the reference voltage at any temperature other than the reference temperature is obtained by performing the back substitution of (9) and (10) into (7). After some rearrangements, the result becomes [18,19]

$$V_{ref} = V_{G0} + (m-1) \cdot \frac{k \cdot T}{q} \cdot \left[1 + \ln\left(\frac{T_0}{T}\right)\right] \tag{12}$$

And thus, we have

$$\frac{\partial V_{ref}}{\partial T} = (m-1) \cdot \frac{k \cdot T}{q} \cdot \ln\left(\frac{T_0}{T}\right) \tag{13}$$

The bandgap temperature sensor is a well-known choice for integrated circuits due to its stability and low thermal drift. It uses the predictable variation of the base emitter voltage (V_{BE}) of a bipolar transistor as a function of temperature. The variation can be expressed as [19]

$$V_{BE} = V_{G0} = \left(1 - \frac{T}{T_0}\right) + m \cdot k \cdot T \cdot \ln\left(\frac{T}{T_0}\right) \tag{14}$$

where

- V_{BE} is the transistor/diode base-emitter voltage.
- V_{G0} is the bandgap voltage extrapolated to 0 °K (typically around 1.2 V).
- T is the absolute temperature in kelvins.
- T_0 is a reference temperature (usually 300 °K or 25 °C).
- K is the Boltzmann constant (1.38×10^{-23} J/K).
- m is an experimental adjustment factor (typically close to 2).

Low-power operation is the major advantage of bandgap sensors; they can be directly integrated into modern microcontrollers, such as the nRF52 series from Nordic Semiconductor, located in Trondheim city in Norway, offering internal temperature measurement capabilities [20]. These sensors are used in applications such as processors, power management circuits, and thermal monitoring for microelectronics [21].

Generally, these NTC thermistors are temperature-dependent resistors that show a negative temperature coefficient; that is, their resistance decreases exponentially with an increase in temperature [22]. The relationship between resistance R and temperature T is described by Steinhart–Hart's equation [22]:

$$\frac{1}{T} = A + B \cdot \ln R + C \cdot (\ln R)^3 \quad (15)$$

where

- R is the resistance of the thermistor in ohms (Ω).
- A, B, and C are Steinhart–Hart coefficients [22], which are characteristics specific to the bulk semiconductor material over a given temperature range of interest or sensor-specific empirical coefficients obtained by calibration.

  A simplified form, valid for moderate temperature variations, is the Beta equation:

$$T = \frac{\beta}{\ln\left(\frac{R}{R_0}\right) + \frac{\beta}{T_0}} \quad (16)$$

where

- T_0 is a reference temperature (usually 25 °C or 298.15 °K).
- R_0 is the resistance of the thermistor at T_0.
- β is the Beta coefficient of the thermistor (typical between 3000 K and 5000 K).

A, B, and C are experimental coefficients defined in [23]. NTCs are used in applications needing precision temperature measurement such as battery systems, medical sensors, and IoT devices [24]. NTC thermistors are usually more accurate than bandgap sensors but require calibration and more complicated readout circuits [25].

Temperature sensors are primary components in an electronic environment, depending on whether an application needs internal or external sensors. Whenever a forbidden bandgap sensor serves for thermal monitoring in most MCUs, NTCs give highly accurate measurements for sensitive applications. Selection therefore depends on considerations like accuracy, power consumption, and the operating temperature range required.

HY0020 [10] is an SoC developed by FDK Corporation [26], which is a Japanese company. A Nordic Semiconductor nRF52 series MCU resides within the HY0020. This MCU integrates an ARM Cortex-M4 processor with an FPU built in, thus allowing for clocking frequencies up to 64 MHz for an optimum performance-to-power tradeoff. BLE 5.0 connectivity is also available with a BLE antenna surrounding the chip: 512 kB flash memory, 64 kB RAM memory, and an operating voltage of 3.3 V [10]; it also has the dimensions 3.5 × 10 × 1 mm. Security hardware for BLE data encryption beyond the reach of ordinary users operates within the security domain of HY0020—with AES-128-bit data encryption being the specific algorithm. On the nRF52 microcontroller, energy-efficient operation is a key requisite, since it is targeted for battery-powered devices and has the following modes:

- Active Mode:
  - Full working condition;
  - BLE transmission of nominal current around 5.3 mA.
- Sleep Mode:
  - Fast wake-up;
  - Reduced current consumption in a small μA range.
- System OFF Mode:
  - Completely off;
  - Nearly zero current, consuming only 0.3 μA.

The MCU has an internal temperature sensor built right into the silicon of the chip. Important for various applications of the HY0020, it acts either as an auxiliary sensor or as a means of monitoring the module's operating conditions. Some operating parameters for the temperature sensor are as follows:

- Measurement range: About −40 °C to +85 °C, which is sufficient for extreme environments.
- Resolution: Typically 0.25 °C for a configuration of the 12-bit Analog Digital Converter (ADC).
- Accuracy: Typically ±1 °C under normal operating conditions.
- Low power: Designed to be highly efficient, it allows for the occasional measurement without a significant impact on the overall consumption of the device.

The internal temperature sensor works by measuring the voltage change in circuits that respond to thermal change on the chip (bandgap reference circuit). The signal is converted by the internal ADC into digital values that are read depending on the firmware developed.

2.2. Relevant Research

The Internet of Things (IoT) is characterized by ongoing growth and innovation. It has evolved from its initial stage of basic connected devices into a sophisticated ecosystem of interconnected sensors, devices, and platforms. Temperature monitoring is a critical aspect of IoT applications, especially in logistics, healthcare, and environmental monitoring. Accurate and reliable temperature data are essential for preserving the integrity of sensitive products, ensuring safety, and optimizing processes.

In the context of IoT temperature monitoring, various systems have been developed to address the challenges of real-time data collection, low-power operation, and sensor integration. These systems leverage advanced technologies such as embedded sensors, wireless communication protocols, and cloud-based analytics to provide precise and efficient temperature monitoring solutions. Achieving low-power operation is crucial for extending the autonomy of these systems, making them more practical and sustainable for long-term use.

Several studies related to the theme under study in this paper have been conducted.

James Prosper [27] explored the integration of smart thermal monitoring systems with the IoT for temperature sensing in rotating equipment. It leverages advanced wireless sensors, edge computing, and cloud analytics to provide real-time insights into thermal variations in industrial machinery. The study discusses the use of various wireless communication protocols and energy harvesting techniques for self-powered sensors. The work focuses on industrial applications and the use of various types of sensors, which could complement our system's use of specific sensors for precise temperature monitoring.

Prediction algorithms of thermal effects were emphasized in the study Ref. [28], where real-time prediction algorithms were applied in validation with the use of the MCUXpresso tool for operative treatment on a Freescale embedded sensor board, wherein it set up sensor programming to monitor real-time temperature. Again, like our system, it was used to monitor temperature in real time using embedded sensors. However, their work emphasizes predictive algorithms for thermal effects, which could complement our system's capabilities.

In Ref. [29], Ellie Gabel explored real-time temperature control systems in urban environments, leveraging IoT technology to collect and analyze data for precise climate management. The work highlights the use of advanced analytics and machine learning to optimize energy efficiency and improve urban living conditions. The system deploys sensors across various infrastructures to gather real-time data on temperature, humidity, and energy usage. The system is similar in providing real-time monitoring and cloud-based analytics. It also emphasizes wireless connectivity and AI-driven insights, which could be an enhancement to our system's BLE connectivity.

Maria Malits, Igor Brouk, and Yael Nemirovsky [30] investigated temperature sensing circuits realized in CMOS silicon-on-insulator (SOI) technology. Their approach uses MOSFET threshold voltage (Vt) extractor circuits for accurate on-chip temperature measurement. The circuits are designed for low power consumption and high accuracy, making them suitable for analog and mixed-signal designs. Their work is highly relevant, as it focuses on integrating temperature sensors with chips, like our use of HY0020 SoC. It emphasizes low power consumption and high accuracy, aligning well with our system's goals.

In Ref. [31], the authors used low-cost sensors and an ESP32 microcontroller to provide real-time monitoring and predictive maintenance. The system was implemented in a photovoltaic solar plant and emphasized remote updates and centralized data visualization. Their work is relevant for integrating multiple sensors on a single chip, like our system's integration of HY0020 and Si7020-A20 sensors. It emphasizes reducing system complexity and enhancing performance.

The study Ref. [32] was conducted to analyze the design and implementation of a temperature monitoring and automatic fan control system based on the Internet of Things. The system Ref. [32] employed an ESP32 Wi-Fi module, a DHT11 temperature sensor, and a transistor for controlling the fan. The fan speed changes with temperature in real time, offering utility, comfort, and energy-saving benefits. The study stresses the precise temperature measurement and timely fan control algorithms of the system. Like our system, it focuses on real-time monitoring and uses IoT technology. However, it emphasizes automatic fan control rather than continuous temperature monitoring for tracking systems.

The main advantage of our system lies in its low-power operation, dual-sensor integration, and cost-effectiveness. This combination ensures high-precision temperature measurements with thermal redundancy, enhancing data reliability while maintaining affordability. These features make the system particularly suitable for applications requiring continuous and reliable temperature monitoring, such as logistics and tracking systems.

Moreover, the system's energy-efficient design provides extended autonomy, making it practical and sustainable for long-term use in remote or resource-constrained environments. While other systems may offer various benefits, our focus on power efficiency and sensor redundancy gives it a unique edge in specific cases where reliability and longevity are critical.

In Table 1, we summarize relevant related works.

Table 1. Summary of the relevant research discussed.

Article	Cost	Effectiveness	Low-Power Operation	Power Consumption	Other Important Characteristics
[32]	Low (Approx. EUR 10–15)	Effective for real-time monitoring and automatic fan control	Moderate	Active Mode: ~160 mA, Sleep Mode: ~10 µA	Focus on automatic fan control, user convenience, and energy efficiency
[29]	High (EUR 1000),	Highly effective; uses advanced analytics and machine learning for precise control	Moderate	Varies widely depending on the scale and components used	Suitable for large-scale urban environments; integrates multiple data sources
[30]	Moderate (Approx. EUR 50–100)	Highly effective; accurate on-chip temperature measurement	High	Active Mode: ~30 µW	Suitable for analog and mixed-signal designs; no need for calibration
[31]	Low (Approx. EUR 20–30)	Effective for monitoring in photovoltaic systems	Moderate	Active Mode: ~160 mA, Sleep Mode: ~10 µA	Focuses on sustainability, remote updates, and centralized data visualization
[27]	High (Approx. EUR 500)	Highly effective; accurate and reliable measurements for industrial settings	Moderate	Varies depending on sensor type and communication protocol	Uses various wireless communication protocols; suitable for harsh environments
[28]	Moderate (Approx. EUR 50–100)	Effective for real-time temperature monitoring and prediction	High	Active Mode: ~5 mA, Sleep Mode: ~1 µA	Emphasizes predictive algorithms for thermal effects

This work	Low (EUR 20)	Highly effective; dual-sensor integration ensures reliability	High	Active Mode: ~5.3 mA, Sleep Mode: ~few μA, System OFF Mode: ~0.3 μA	Cost-effective, real-time monitoring; suitable for tracking systems

There are many reasons behind the choice to design an internal or temperature-dedicated sensor instead of ordering one externally. Among these are to obtain point data with high thermal constancy while somehow having a direct interfacing ability with the HY0020 microcontroller without requiring additional external components. The design can also run for multi-year cycles on a non-rechargeable battery, with an optimum layout to promote thermal encapsulation. Avoiding the utilization of external sensors leads to the reduction of the PCB area and Bill Of Materials (BOM), as well as mounting and soldering failures, such that it is then very easy to go through Electromagnetic Compatibility (EMC) certification and establish good thermal robustness. In Table 2, we present other bandgap temperature sensors.

Table 2. Summary of other bandgap temperature sensors.

Sensor	Minimum Voltage (V)	Typical Consumption	Thermal Range (°C)	Observations
LM35 [33]	4–30	~60 μA	−55 to 150	Analog requires ADC
TMP117 [34]	≥1.8	~3 μA (sleep), 150 μA (active)	−55 to 150	Digital; accuracy ±0.1 °C
MAX31855 [35]	≥3	~1.5 mA	−200 to 1350	Only for K thermocouples
MCP9700 [36]	2.3–5.5	~6 μA	−40 to 125	Analog
HDC2080 [37]	≥1.62	~0.55 μA (sleep)	−40 to 125	Temperature and humidity
AD590 [38]	≥4	200 μA	−55 to 150	Current proportional to temperature

Being commercial sensors, precision notwithstanding, they feature limiting factors when working in ultra-low-power IoT systems under extreme environments. As shown in the table, typical problems relate to high continuous current consumption, requirements of support circuitry (e.g., ADCs, regulators, and filters), large size and cost, susceptibility to interference and heating from their use, and long stabilization time after wake-up, to name a few.

The TMP117 [34] and MAX31855 [35] sensors can be highly accurate and come fully factory-calibrated; however, the HY0020's internal sensor strikes the best power-performance balance with ruggedness. This enables full optimization of the design for ultra-intermittent duty cycles, which completely removes external dependencies.

The HY0020 integrates a PTAT sensor using matched transistors along with an internal reference to provide low noise, good thermal stability, and repeatability. Calibration data are stored in ROM and used for digital correction in firmware. It achieves a very fast readout time of under 5 ms, turning on just for brief read cycles, and draws nanoamp currents while in sleep mode. Being integrated inside the SoC eliminates external components, improving EMI immunity and voltage stability. The internal calibration results in a well-known thermal error curve, which can be compensated with regression models at the firmware level. Lastly, monolithic integration means that thermal loss to the substrate is minimized, thus enabling reliable measurements in systems with thermal isolation.

3. Materials and Methods

This section proceeds subdivided into subsections; it offers a concise, precise description of the experimental system, a description of the different scenarios, the hardware integration, and algorithms developed for the gateway and the node.

3.1. System Implementation and Hardware Setup

Figure 2 illustrates the system architecture used in the experiment**.** The system comprises the HY0020 [10] System-on-Chip (SoC), referred to as the IoT-Temp Node, for which a custom printed circuit board (PCB) was developed. This PCB includes a coin cell battery holder and integrates an external temperature sensor (Si7020-A20 [12]) for comparative analysis. A Wi-Fi gateway, based on a Raspberry Pi 4 [14], is positioned externally to the IoT-Temp Node and is responsible for forwarding the collected data to an IoT cloud platform [39].

The Raspberry Pi 4 [14], used in this experiment as a gateway, is a single-board computer running Ubuntu Server 22.04.4 LTS from a 32 GB microSDHC card. It serves as an intermediary between the IoT-Temp Node and the IoT cloud platform (Sensefinity Cloud [39]). Communication between the IoT-Temp Node and the gateway is established via a Bluetooth Low Energy (BLE) network, while the gateway connects to the cloud using Wi-Fi.

Raspberry Pi 4 was chosen over the ESP32 (Espressif Systems, Shanghai, China) [40] for better performance, reliability, and scalability for demanding BLE and Wi-Fi applications. Unlike the ESP32 internal temperature sensor, which is unreliable due to lack of calibration and internal heating, the HY0020 device, communicating with the Raspberry Pi over BLE, is factory-calibrated and hence thermally precise. In terms of technology, the Raspberry Pi 4 comes with a robust four-core ARM Cortex-A72 CPU, up to 8 GB of RAM, and a full Linux OS. This enables BLE scanning to run alongside local data processing and secure cloud communication via Hypertext Transfer Protocol Secure (HTTPS) or Message Queuing Telemetry Transport (MQTT) with Transport Layer Security (TLS). It supports multi-tasking, better coexistence of interfaces (BLE/Wi-Fi), persistent logging, Over-The-Air (OTA) updates, and containerization (e.g., Docker). The ESP32, in contrast, being limited in processing power and memory, fits better for simpler, ultra-low-power use cases involving fewer BLE devices and possibly looser networking requirements.

Although Figure 2 depicts multiple IoT-Temp Nodes and gateways to illustrate the system's scalability, the experimental setup involved only one IoT-Temp Node and two identical gateways placed at different locations within the laboratory.

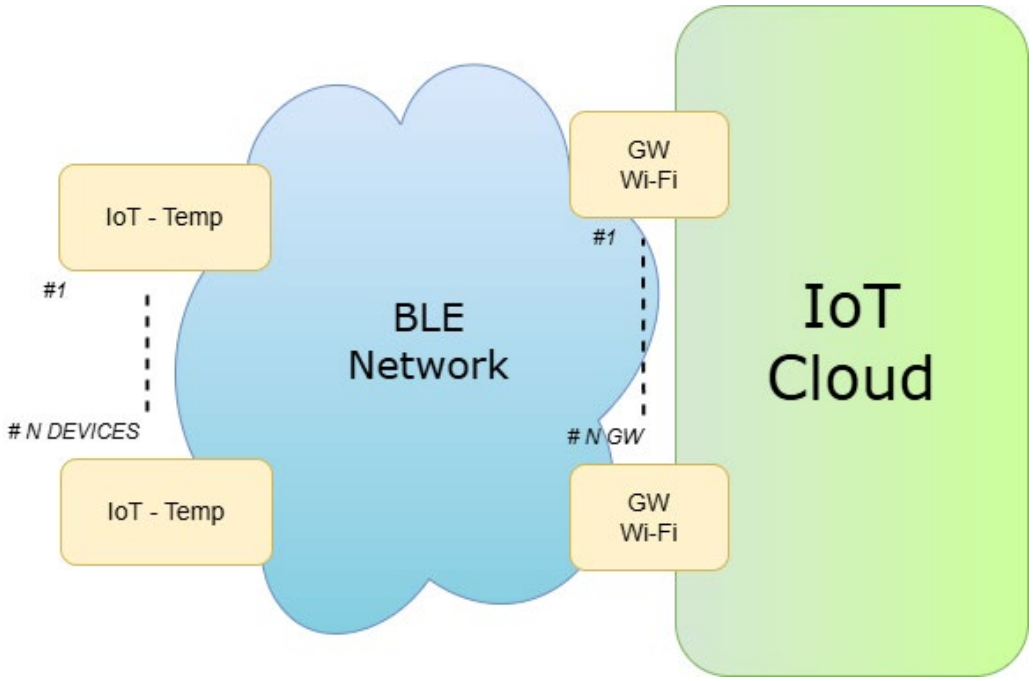

Figure 2. System architecture.

3.2. Hardware Integration

Figure 2 describes an established design study, with an illustration provided (Figure 3) and its subsequent realization regarding PCB layout. Figure 3 shows the PCB layout that includes HY0020 SoC, Si7020-A20 temperature sensor (external to HY0020), and a holder for coin cell battery. The PCB has 3.4 × 1.6 × 0.8 cm dimensions (Figure 4). Figure 5 shows a 3D view of the PCB.

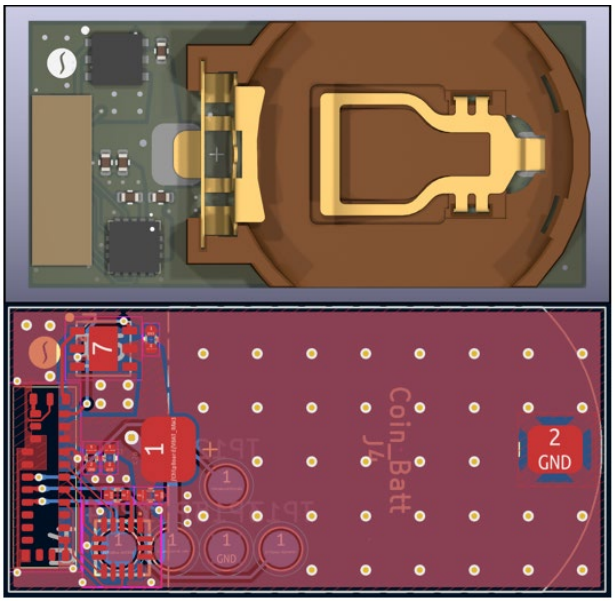

Figure 3. PCB layout of IoT-Temp Node.

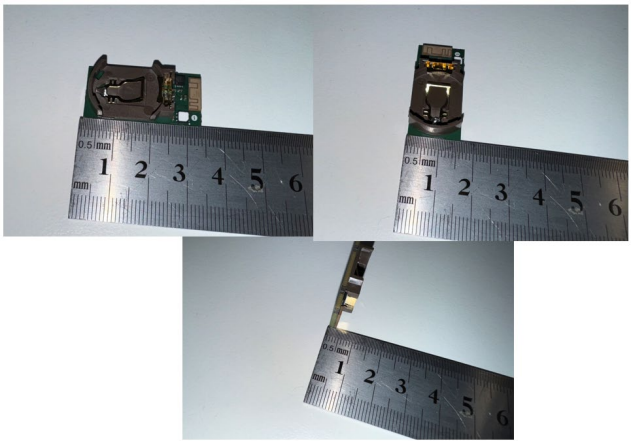

Figure 4. IoT-Temp Node with dimensions.

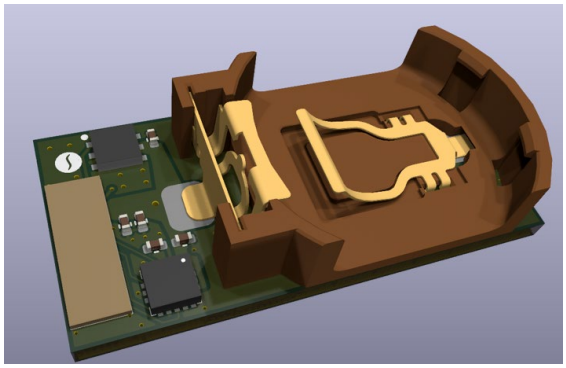

Figure 5. IoT-Temp Node 3D view.

Figure 6 shows the final replicated prototype, which had been subassembled, installed into an enclosing chamber, and directed toward the experiment (with box dimensions).

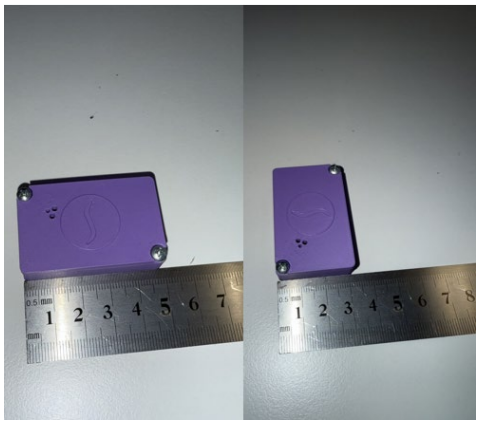

Figure 6. Final prototype (IoT-Temp Node), with box dimensions.

Figure 7 shows the gateway used in our experiment based on Raspberry Pi 4 and power supply circuits to convert 230 VAC to 5 VDC. While traditionally the preference is for fuses in the realms of low-power and microelectronics applications such as Raspberry Pi 4, circuit breakers present several accrued advantages when seen from a wider project perspective, as shown in Figure 7. The Raspberry Pi rarely works in isolation; it is most often fused with different sensors, actuators, power drivers, and industrial systems. Thus, protection must be beyond the mere overcurrent regime. Circuit breakers are excellent in providing several benefits, including instant disconnection in the event of a fault, improved safety, and easier maintenance, all of which can be handy if the location is tough to reach or if the environment calls for continuous use. Circuit breakers, unlike fuses, allow for quick visual diagnostics and can be reset, thus reducing downtime and increasing system availability. Their mounting into standard Deutsches Institut für Normung (DIN) rails or modular enclosures facilitates a strongly scalable and professional system layout able to be maintained, whether in educational, laboratory, or industrial environments. They are compact enough to be used in low-current applications, aligning well with maintenance- and safety-oriented design principles. Thus, in low-power applications, circuit breakers can deliver a technically better and durable protection choice.

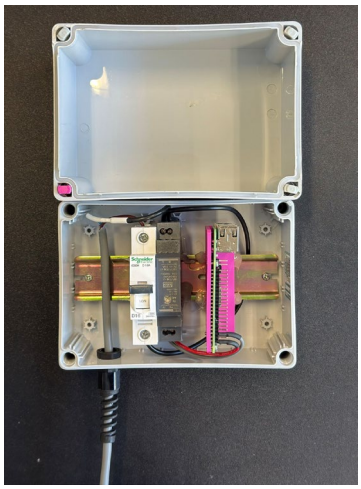

Figure 7. Gateway—Raspberry Pi 4.

3.3. Algorithms Developed

Firmware was developed in the C programming language for the HY0020 SoC within the IoT-Temp Node. Its primary function is to read temperature data from both the internal and external sensors, package the readings into a payload, and transmit this payload over a Bluetooth Low Energy (BLE) network. The IoT-Temp Node scans for a valid BLE gateway (Raspberry Pi 4) and, upon discovery, sends the payload for further processing. The gateway receives the BLE payload, processes the data, and forwards them to the IoT cloud platform. The operational flow of the IoT-Temp Node is illustrated in Figure 8.

The Raspberry Pi 4 functions as a BLE server, continuously listening for incoming data from the IoT-Temp Node. Upon receiving a payload, it processes the data by converting them into a structured format, such as JSON, which is suitable for cloud-based systems. The formatted data are then transmitted to the cloud.

Data transmission to the cloud is performed using the HTTPS protocol, ensuring secure end-to-end communication. This is achieved by initiating an HTTPS request to a RESTful API hosted on the Sensefinity cloud platform [39].

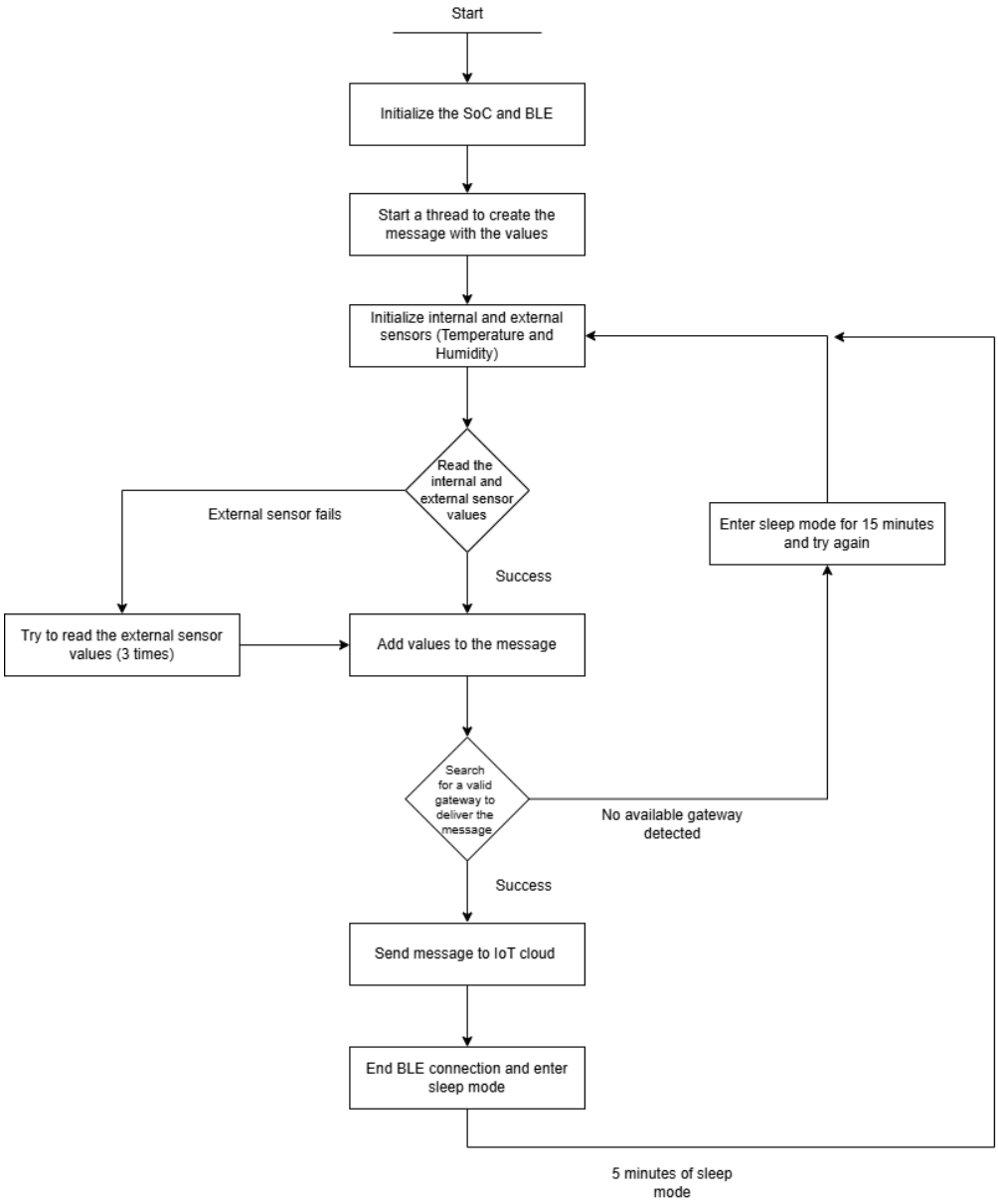

Figure 8. Flowchart of IoT-Temp Node.

The algorithm presented in Figure 8, in essence, describes how an embedded system works on an SoC, providing BLE communications for environmental monitoring through temperature and humidity data collection on an internal/external basis. The system is designed for autonomous and power-saving operation between active and deep sleep mode depending on its operating conditions.

The procedure starts with the configuration and activation of the SoC and BLE interface, which are basic elements that facilitate wireless connectivity to IoT gateways. In this initial stage, a thread dedicated to data-message assembly is created. This message would be regarded as the unit of information intended to be sent to the target platform, usually the database or cloud application. Next, the sensors responsible for measuring environmental variables are initialized. The system considers two kinds of sensors: an internal one, integrated within the architecture of the HY0020, and an external one, connected via some digital interface (I2C). The sensors are read in a sequential manner, and in case of communication failure, up to three read attempts might be made with the external sensor. This retry mechanism maximizes the chances that collected data are reliable while preventing the system from blocking operations in cases of continuous failure.

In case the sensors are read successfully, the values obtained are immediately included in the already created message. This complete message is then prepared for transmission, requiring the detection of a nearby valid gateway. The system searches actively for such a gateway. When no receiving device is found, the system immediately goes to sleep for a period of 15 min and starts another attempt at reading the sensors. This also helps in reducing energy spent during non-productive and repeated communications.

If a valid gateway is present, the message is sent through the BLE connection. This transmission is confirmed, and then the connection is cut off to save energy, followed by a shorter sleep period of 5 min. That period allows for a balance between periodicity of data collection and system energy autonomy.

At the end of this sleep cycle, the system restarts from the sensor reading stage, thus completing the entire process cyclically. This circular logic guarantees continuous operation and sustainability; hence, it is very suitable for applications in remote locations with difficult access to energy sources or even integrated solutions into smart cities.

Low-power IoT system best practices are characteristically illustrated by this type of algorithm, merging efficient energy management, sensor fault tolerance, and adaptive communication logic with available infrastructure. Due to its modularity, the algorithm (Algorithm 1—IoT-Temp Node) is easily modifiable or extendable to accommodate new sensors, other communication protocols, or edge computing techniques.

Algorithm 1: IoT-Temp Node.

1. Initialize HY0020 SoC.
2. Initialize BLE.
3. Create Thread for Composing Data Message.
4. Initialize Temp. and Humidity Internal Sensor.
5. Initialize Temp. and Humidity External Sensor.
6. Attempt to Read Value from Internal Sensor.
7. Attempt to Read Value from External Sensor.
    - 7.1 If fail:
        - 7.1.1 Repeat Read for 3 times
        - 7.1.2 If still fails, ignore the external sensor values and continue with the data available
    - 7.2 If reading is successful: add internal and external data to message
8. Search Valid Gateway to Send to
    - 8.1 If no gateway is found, sleep for 15 min, then restart from 4.

8.2 If there is gateway: Send the message to the cloud via BLE.
9. Interrupt BLE connection.
10. Go to sleep for 5 min.
11. Go back to step 4.

3.4. Test Scenarios

The experiment was conducted under two distinct environmental conditions: room temperature (laboratory conditions) and a low-temperature environment inside a standard household refrigerator. This was a test on the internal temperature sensor integrated into the System-on-Chip (SoC) HY0020, whereby its measurements were compared against those from two precise external reference sensors known for thermal stability and accuracy.

The primary reference sensor used was the Si7020-A20, which, according to the manufacturer's datasheet, has an accuracy of ±0.4 °C. This sensor was externally mounted on the custom-designed printed circuit board (PCB) that also housed the HY0020 SoC. Its role was to serve as a benchmark for assessing the accuracy of the internal sensor.

Additionally, a second external sensor, the DHT22, was included in the analysis. This sensor operated independently of the IoT-Temp Node and is specified by the manufacturer to have an accuracy of ±0.5 °C. Its inclusion allowed for a broader comparison across different sensor technologies and accuracy classes.

The aim of this experimental setup was to compare the accuracy of the internal HY0020 sensor with that of the external Si7020-A20 and DHT22 sensors under both stable and dynamic thermal conditions. This comparison provides insight into the reliability and suitability of the internal sensor for thermal monitoring in IoT applications, particularly in scenarios characterized by significant temperature variation.

4. Results

This section contains different subsections; first, it deals with the application of the IoT-Temp Node under two scenarios. Section 4.2 describes the energy consumption of the IoT-Temp Node.

4.1. Experiment Scenarios

The first experiment tested room temperature in our laboratory using the PCB that included the HY0020 internal sensor and Si7020-A20 as external sensors. We added in this experiment another device that used a DHT22 temperature sensor. For this experiment, we measured the temperature over 12 h (720 min), as shown in Figure 9.

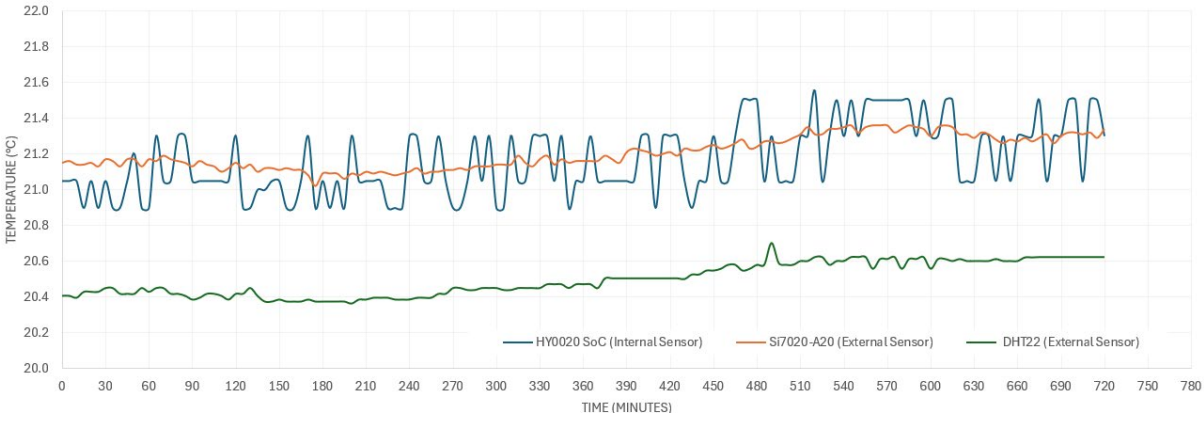

Figure 9. Room temperature recorded in the laboratory over a 720-minute period. Detailed temperature values are provided.

As illustrated in Figure 9, the temperature trends recorded over a 720-minute period were generally consistent across the three sensors used. Notably, the internal sensor (HY0020) and the external sensor (Si7020-A20) exhibited closely aligned readings, with the external sensor demonstrating greater stability over time. This enhanced stability is attributed to its higher sampling frequency—400 ksps for the Si7020-A20 compared to 200 ksps for the HY0020—which allows for more frequent and precise data acquisition.

The difference in accuracy between these two sensors and the DHT22 is also evident, highlighting the superior performance of the HY0020 and Si7020-A20 in capturing temperature variations.

Figure 10 shows the temperature error between the internal sensor (HY0020) and external sensor (Si7020-A20), where we used the external sensor as the value reference.

Figure 10. Temperature error between internal sensor (HY0020) and external sensor (Si7020-A20), using external sensor as value reference. Detailed temperature error values are provided.

Most of the observed errors fell within the range of −0.3 °C to +0.3 °C, indicating good relative accuracy of the internal sensor. Minor periodic oscillations of very small amplitude were detected, which may be attributed to stable environmental influences or inherent sensor limitations such as resolution or latency. Importantly, there is no evidence of systematic drift over time; the errors appear to have been randomly distributed around zero, suggesting the absence of significant bias.

A slight predominance of positive errors was noted during the initial 200 s. While a few moderate outliers were present, they remained within acceptable limits for low-cost sensor applications. Overall, the temporal stability of the internal sensor was satisfactory, with no substantial fluctuations observed.

Potential causes for the observed discrepancies include calibration differences, sensor response time, physical placement, and resolution. The average error was calculated to be approximately 0.041 °C, indicating that, on average, the internal sensor slightly overestimated the temperature compared to the reference sensor. The average absolute error was around 0.138 °C, reflecting the typical magnitude of deviation regardless of direction. The standard deviation of the error was approximately 0.156 °C, representing the variability of the error over time.

Collectively, these error metrics fall within acceptable bounds for continuous temperature monitoring in applications such as food safety or healthcare, where moderate precision is sufficient.

In the last experiment, we used a home refrigerator with a temperature between 6 °C and −2 °C.

For this experiment, we measured the temperature by over a period of 4 h and 30 min (270 min), as shown in Figure 11.

Looking at Figure 11, from 0–270 min, the temperatures were monitored by sensors every 5 minutes. Reference readings were collected from the onboard sensor (HY0020 SoC), the external reference sensor (Si7020-A20), and the external sensor (DHT22), with notable deviations observed at minute 90, when the refrigerator door was opened and the sensors were temporarily removed. For instance, the average error using the HY0020 SoC sensor compared to the reference Si7020-A20 was about −0.17 °C, whereas the standard deviation and average absolute error were 2.66 °C and 1.74 °C, respectively. This indicates that although the average error was relatively small (slightly negative), the variability of the error was substantial during the period of exposure to ambient conditions. The average error compared to the DHT22 was more positive, which suggests that the HY0020 was continuously reading lower values than the DHT22, especially after 90 min, when sharp peaks appeared in the readings of the DHT22.

Prior to the 90-minute mark, the internal sensor's errors remained relatively stable, oscillating within a narrow band of approximately ±1 °C. The abrupt rise in the HY0020's readings, which surged to 14.5 °C, happened after opening the fridge door to the free outside environment, during which the external sensors recorded temperatures of 13.5 °C (Si7020-A20) and 5.3 °C (DHT22), respectively. These discrepancies can be attributed to differences in thermal response and sensor placement, which led to temporary deviations from expected values.

Once the sensors were returned to the refrigerator, the readings gradually stabilized. The HY0020 showed, however, more oscillatory behavior compared to the external sensors. This was further validated by the statistical data: a low average error coupled with a high standard deviation suggests sporadic error spikes, reducing reliability under rapidly changing thermal conditions.

The external sensors, particularly the Si7020-A20, showed good agreement with the HY0020, indicating similar thermal response characteristics. In contrast, the DHT22 exhibited significant deviations and sharp peaks after the 90-minute mark, with differences reaching up to 6.8 °C, suggesting a slower response to the temperature drop after being returned to the refrigerator.

Overall, the experiment highlights the pronounced impact of sudden environmental changes—such as sensor removal and door opening—on temperature readings. The HY0020 SoC sensor demonstrated high thermal sensitivity but also exhibited momentary fluctuations in error due to thermal disturbances. These errors eventually returned to acceptable levels, albeit with continued oscillations. Such behavior should be considered during calibration or validation for critical applications.

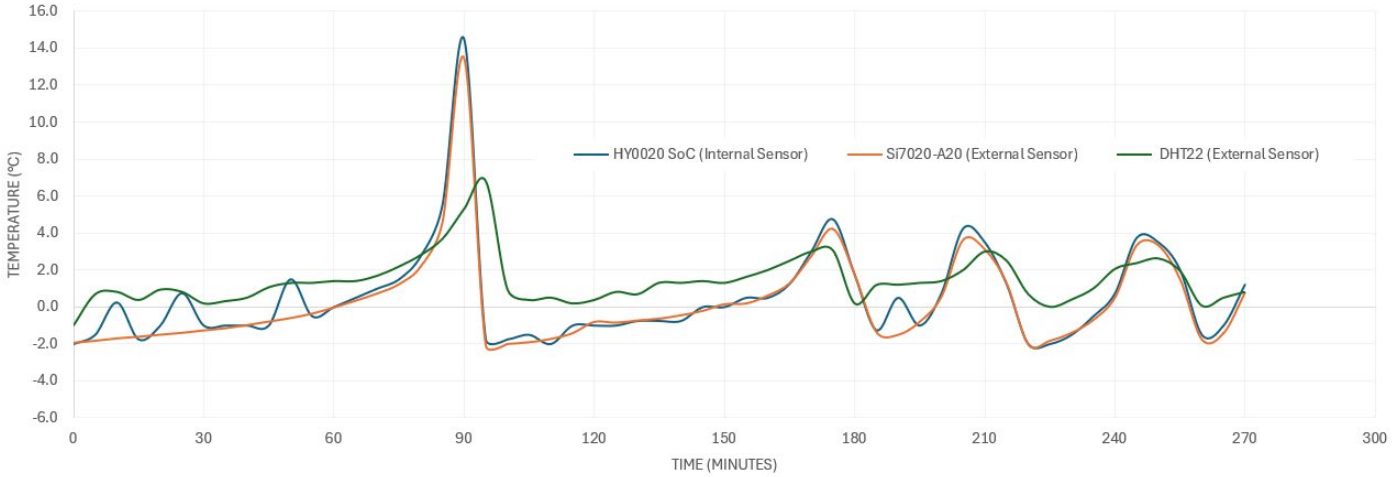

Figure 11. Home refrigerator temperature recorded over a 270-minute period. Detailed temperature values are provided.

Looking at Figure 12, the evaluation of the data gathered over a span of 270 min between the internal sensor and external reference sensor at 5-minute intervals indicates that the performance was stable overall, though some significant drift events were observed.

The average error was about −0.36 degrees Celsius, indicating that the internal sensor tended to underestimate the actual temperature relative to the external reference sensor. This negative bias suggests that under normal use, without further calibration, the internal sensor will produce readings slightly below the true temperature. The standard deviation of the errors was calculated at 0.61 °C, indicating moderate variability throughout the measurement period, which is a typical resulting outcome in environments subject to minor thermal fluctuations. The mean absolute error was approximately 0.47 °C, reflecting excellent average precision of the internal sensor despite small deviations from the reference.

Although the overall statistical stability remained good, certain time points exhibited relatively significant deviations. The biggest errors were noticed at 10, 25, 50, and 190 min. Their values were −1.9 °C, −2.1 °C, −2.1 °C, and −2.0 °C, respectively. These deviations were observed at just some specific points, very briefly (initially), and are attributed to sudden environmental changes or delayed thermal response of the internal sensor.

A particularly relevant event took place at 90 min when the refrigerator door was opened. This caused a brief thermal disturbance, which is evident in the data: an error of −1.0 °C was recorded, indicating a rapid temperature drop detected by the internal sensor during thermal compensation. This behavior highlights the sensor's sensitivity to abrupt environmental changes, which, from a dynamic response perspective, may be considered a positive attribute.

While several error spikes were noted, they were contextually explainable, such as the disturbance caused by the sudden door opening. For applications where minimal variation is critical, point calibration or software-based compensation is recommended to address the consistently observed negative bias in the internal sensor's readings.

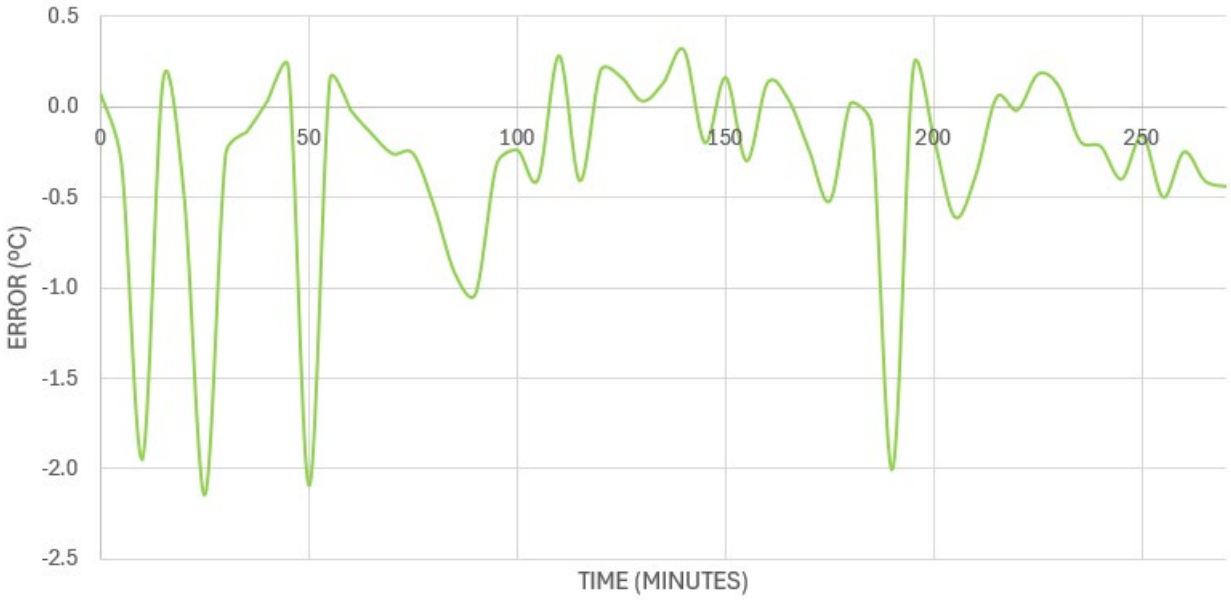

Figure 12. Home refrigerator temperature error between internal sensor (HY0020) and external sensor (Si7020-A20), using external sensor as value reference. Detailed temperature error values are provided.

Our system demonstrated high accuracy within its intended operational range (e.g., average error of 0.041 °C at room temperature and −0.36 °C in refrigeration). It is primarily designed for general-purpose and operational level monitoring scenarios, where deviations within ±0.5 °C are acceptable.

4.2. Energy Consumption

Energy consumption testing of the IoT-Temp Node device was conducted using the Joulescope JS220 meter (Joulescope, Rockville, MD, USA) [41] over a continuous period of approximately two days (2:00:31:48), as shown in Figure 13.

In this measurement, the Si7020-A20 external sensor was intentionally disabled via firmware to isolate and measure the baseline energy consumption of the core system The Joulescope interface recorded a total accumulated consumption of 525.622 μAh. The current profile exhibited intermittent bursts of high activity mixed with extended periods of minimal current draw—behavior characteristic of IoT systems engineered for ultra-low-power operation. The average current measured was approximately 0.01727 mA, confirming the system's efficiency in standby mode.

A critical aspect of validating the system's suitability for real-world deployment is the estimation of operational autonomy, particularly in scenarios where energy availability directly impacts performance. To this end, the autonomy of the IoT-Temp Node was estimated using the recorded average current consumption, with the Si7020-A20 sensor disabled via firmware to isolate the base system's power profile. Assuming a CR2477 3 V lithium battery with a nominal capacity of 1000 mAh and an average current draw of 0.01727 mA, the device is projected to operate for approximately 6.6 years. This result underscores the node's potential for long-term deployment in energy-constrained environments, even under minimal power configurations.

Figure 13. Energy consumption recorded for the IoT-Temp Node over 2 days.

5. Conclusions

This work presented the design and evaluation of IoT-Temp Node, a compact, low-power temperature monitoring system based on the HY0020 SoC. The system was tested under both stable and dynamic thermal conditions—room temperature and refrigeration—to assess its accuracy, responsiveness, and energy efficiency. The results confirmed that the internal sensor delivers precise and stable readings, with deviations well within ±0.5 °C, even during abrupt environmental changes.

At room temperature, the internal sensor exhibited an average error of just 0.041 °C and an average absolute error of 0.138 °C, with minimal drift. Under refrigeration conditions, despite more dynamic thermal variations, it maintained a mean error of −0.36 °C and an absolute error of 0.47 °C. These results confirm the sensor's high accuracy and reliability across a range of operating conditions.

A key contribution of this work lies in the design and validation of a complete, low-power monitoring platform that enables and demonstrates the internal sensor's advanced capabilities, including real-time parameterization, thermal profiling, cross-validation, and background diagnostics. This integrated approach not only confirms the sensor's standalone performance but also highlights the value of the system as a versatile tool for smart monitoring in critical applications such as cold-chain logistics, pharmaceutical transport, and organ preservation.

The system also demonstrated exceptional energy efficiency, averaging just 0.01727 mA in consumption, which translates to an estimated battery life of 6.6 years on a standard CR2477 cell. Combined with its compact form factor and low cost, this makes it ideal for long-term deployments in space- and power-constrained environments.

Compared to existing solutions, the IoT-Temp Node offers, in this way, a unique combination of precision, autonomy, and diagnostic intelligence using commercially available components. In future work, we aim to explore adaptive calibration, optimized wireless communication, and deeper integration with digital traceability frameworks such as the DPP, further expanding its impact in sustainable and transparent supply chains.

Author Contributions: Conceptualization, L.M.P., J.F. and R.M.; methodology, L.M.P., J.F., J.M. and R.M.; software, L.M.P. and R.M.; validation, L.M.P. and J.M.; formal analysis, L.M.P. and J.M.; investigation, L.M.P., J.M., J.F. and R.M.; resources, L.M.P., J.F., J.M. and R.M.; data curation, L.M.P., J.F., R.M. and J.M.; writing—original draft preparation, L.M.P., J.F., R.M. and J.M.; writing—review and editing, L.M.P., J.M. and J.N.; visualization, L.M.P., J.F., R.M. and J.M.; supervision, L.M.P. All authors have read and agreed to the published version of the manuscript.

Funding: This research received no external funding.

Data Availability Statement: The raw data supporting the conclusions of this article will be made available by the authors on request.

Acknowledgments: All the authors would like to express their gratitude to the Sensefinity company for making the PCB for SoC-HY0020 for use during the experiments, as well as for the use of the Sensefinity IoT cloud.

Conflicts of Interest: All the authors declare no conflicts of interest.

References

1. FAO. *Food Loss and Waste Reduction*; FAO: Rome, Italy, 2021.
2. WHO. *Temperature Monitoring in the Vaccine Supply Chain*; WHO: Geneva, Switzerland, 2022.
3. UNDP. *Sustainable Cold Chain for Food and Medicine*; UNDP: New York, NY, USA, 2023.
4. UNEP. *Sustainable Production and Consumption Patterns*; UNEP: Nairobi, Kenya, 2020.
5. WEF. *The Future of Smart Logistics and Industry 4.0*; WEF: Geneva, Switzerland, 2021.
6. IPCC. *Climate Change and Food Systems*; IPCC: Geneva, Switzerland, 2019.
7. UNFCCC. *Reducing Carbon Footprint in Global Supply Chains*; UNFCCC: Bonn, Germany, 2022.
8. DPP Portal. About Digital Product Passport. Available online: https://psqr.eu/publications-resources/all-about-dpp/ (accessed on 2 April 2025).
9. European Comission. Available online: https://cirpassproject.eu/wp-content/uploads/2024/03/A2-EC-Michele-Galatola.pdf (accessed on 20 March 2025).
10. HY0020. Available online: https://www.fdk.com/cyber-e/electronic_components/module/hy0020.html (accessed on 22 January 2025).
11. Nordic. Available online: https://www.nordicsemi.com/ (accessed on 10 February 2025).
12. Silicon Labs. Available online: https://www.silabs.com/sensors/humidity/si7006-13-20-21-34/device.si7020-a20-im?tab=specs (accessed on 2 February 2025).
13. Adafruit. Available online: https://www.adafruit.com/product/385 (accessed on 5 March 2025).
14. Raspberry Pi. Available online: https://www.raspberrypi.com/products/raspberry-pi-4-model-b/specifications/ (accessed on 1 March 2025).
15. *Understanding and Interpreting Standard-Logic Data Sheets*; Application Report SNOAA25; Texas Instruments: Dallas, TX, USA, 2004. Available online: https://www.ti.com/lit/ab/snoaa25/snoaa25.pdf (accessed on 9 June 2025)
16. Analog Devices. Chapter 7: Temperature Sensors in Industrial Applications. In *Temperature Sensors—A Tutorial for Engineers*; Analog Devices: Norwood, MA, USA. Available online: https://www.analog.com/media/en/training-seminars/design-handbooks/temperature_sensors_chapter7.pdf (accessed on 5 June 2025).
17. Tsividis, Y. *Operation and Modeling of the MOS Transistor*, 2nd ed.; The Oxford Series in Electrical and Computer Engineering; Oxford University Press: New York, NY, USA, 1999; ISBN 978-0-19-517014-6.
18. Carusone, T.C.; Johns, D.A.; Martin, K.W. *Analog Integrated Circuit Design*, 2nd ed.; Wiley: Hoboken, NJ, USA, 2011; ISBN 978-0-470-77010-4.
19. Jingwen, M.; Tingqian, C.; Cheng, C.; Junyan, R.; Li, Y. CMOS 1.5V bandgap voltage reference. In Proceedings of the 2005 6th International Conference on ASIC, Shanghai, China, 24–27 October 2005; pp. 469–472. https://doi.org/10.1109/ICASIC.2005.1611359.
20. Nordic Semiconductor. *nRF52 Series Reference Manual*; Nordic Semiconductor: Oslo, Norway, 2021. Available online: https://www.nordicsemi.com/ (accessed on 1 June 2025)

21. Maxim Integrated. *Temperature Sensors in Microelectronics*; Maxim Integrated: San Jose, CA, USA, 2019; Available online: https://www.maximintegrated.com (accessed on 2 June 2025)
22. Steinhart, J.S.; Hart, S.R. Calibration Curves for Thermistors. *Deep Sea Res. Oceanogr. Abstr.* **1968**, *15*, 497–503. https://doi.org/10.1016/0011-7471(68)90057-0.
23. Chen, C. Evaluation of Resistance–Temperature Calibration Equations for NTC Thermistors. *Measurement* **2009**, *42*, 1103–1111. https://doi.org/10.1016/j.measurement.2009.04.004.
24. Murata Manufacturing. *NTC Thermistors: Applications and Design Considerations*; Murata Manufacturing: Kyoto, Japan, 2020; Available online: https://www.murata.com/en-global/products/thermistor/index/documents/applicationmanual (accessed on 2 June 2025)
25. Vishay. *NTC Thermistors: Theory and Application*; Vishay Intertechnology: Malvern, PA, USA, 2018. Available online: https://www.vishay.com/en/thermistors/ntc/ (accessed on 2 June 2025)
26. FDK Corporation. Available online: https://www.fdk.com/ (accessed on 10 March 2025).
27. Prosper, J. Smart Thermal Monitoring Systems: IoT-Enabled Temperature Sensing for Rotating Equipment. 2025. Available online: https://www.researchgate.net/publication/390233231_Smart_Thermal_Monitoring_Systems_IoT-Enabled_Temperature_Sensing_for_Rotating_Equipment_1 (accessed on 19 May 2025).
28. Ettahri, O.; Oukaira, A.; Ali, M.; Hassan, A.; Nabavi, M.; Savaria, Y.; Lakhssassi, A. A Real-Time Thermal Monitoring System Intended for Embedded Sensors Interfaces. *Sensors* **2020**, *20*, 5657. https://doi.org/10.3390/s20195657.
29. Gabel, E. Optimizing Urban Climate with Real-Time Temperature Control Systems in Smart Cities. IoT For All. Last Updated: 2 December 2024. Available online: https://www.iotforall.com/optimizing-urban-climate-with-real-time-temperature-control-systems-in-smart-cities (accessed on 19 May 2025).
30. Malits, M.; Brouk, I.; Nemirovsky, Y. Study of CMOS-SOI Integrated Temperature Sensing Circuits for On-Chip Temperature Monitoring. *Sensors* **2018**, *18*, 1629. https://doi.org/10.3390/s18051629.
31. Lisboa, Y.; Santos, L.; Lobato, E.; Fonseca, W.; Silva, K.; Rodrigues, I.; Silva, M. Design and Implementation of a Sustainable IoT Embedded System for Monitoring Temperature and Humidity in Photovoltaic Power Plants in the Amazon. *Sustainability* **2025**, *17*, 2347. https://doi.org/10.3390/su17062347.
32. Resquites, J.; Parrocho, M.; Vinegas, N.; Oquiño, V. IoT-Based Temperature Monitoring and Automatic Fan Control Using ESP32. *Iconic Res. Eng. J.* **2023**, *7*, 35–44.
33. Texas Instruments. LM35 Precision Centigrade Temperature Sensor. Datasheet. 2016. Available online: https://www.ti.com/lit/ds/symlink/lm35.pdf (accessed on 1 June 2025).
34. Texas Instruments. TMP117: High-Accuracy, I2C Temperature Sensor. Datasheet. 2020. Available online: https://www.ti.com/lit/ds/symlink/tmp117.pdf (accessed on 1 June 2025).
35. Analog Devices (Maxim Integrated). MAX31855 Cold-Junction Compensated Thermocouple-to-Digital Converter. Datasheet. Rev. 4. 2011. Available online: https://www.analog.com/media/en/technical-documentation/data-sheets/MAX31855.pdf (accessed on 1 June 2025).
36. Microchip Technology. MCP9700/9700A/9701/9701A—Low-Power Linear Active Thermistor ICs. Datasheet. 2005. Available online: https://ww1.microchip.com/downloads/en/DeviceDoc/21942d.pdf (accessed on 1 June 2025).
37. Texas Instruments. HDC2080: Low Power Humidity and Temperature Digital Sensor. Datasheet. 2018. Available online: https://www.ti.com/lit/ds/symlink/hdc2080.pdf (accessed on 1 June 2025).
38. Analog Devices. AD590: Two-Terminal Temperature Transducer. Datasheet. Rev. E. 2009. Available online: https://www.analog.com/media/en/technical-documentation/data-sheets/AD590.pdf (accessed on 1 June 2025).
39. Sensefinity. Available online: https://www.sensefinity.com/ (accessed on 22 March 2025).
40. Espressif Systems. ESP32 Technical Reference Manual, Version 4.4. 2021. Available online: https://www.espressif.com/sites/default/files/documentation/esp32_technical_reference_manual_en.pdf (accessed on 4 June 2025).
41. Joulescope. Available online: https://www.joulescope.com/products/js220-joulescope-precision-energy-analyzer (accessed on 22 April 2025).